Hybrid WENO schemes with different indicators on curvilinear grids

Gang Li & Jianxian Qiu

Springer

Springer

Hybrid WENO schemes with different indicators on curvilinear grids

Gang Li · Jianxian Qiu

Abstract In {*J. Comput. Phys.* 229 (2010) 8105-8129}, we studied hybrid weighted essentially non-oscillatory (WENO) schemes with different indicators for hyperbolic conservation laws on uniform grids for Cartesian domains. In this paper, we extend the schemes to solve two-dimensional systems of hyperbolic conservation laws on curvilinear grids for non-Cartesian domains. Our goal is to obtain similar advantageous properties as those of the hybrid WENO schemes on uniform grids for Cartesian domains. Extensive numerical results strongly support that the hybrid WENO schemes with discontinuity indicators on curvilinear grids can also save considerably on computational cost in contrast to the pure WENO schemes. They also maintain the essentially non-oscillatory property for general solutions with discontinuities and keep the sharp shock transition.

Keywords WENO reconstruction · Upwind linear reconstruction · Troubled cell indicator · Hyperbolic system of conservation laws · Hybrid schemes · Curvilinear grid

Mathematics Subject Classifications (2010) 65M60 · 65M99 · 35L65

G. Li
School of Mathematical Sciences, Qingdao University,
Qingdao, Shandong, 266071, Peoples's Republic of China
e-mail: gangli1978@163.com

J. Qiu (✉)
School of Mathematical Sciences, Xiamen University,
Xiamen, Fujian, 361005, Peoples's Republic of China
e-mail: jxqiu@xmu.edu.cn

1 Introduction

In this paper, we extend the hybrid weighted essentially non-oscillatory (WENO) scheme with different indicators, which were originally investigated by Li and Qiu [11] for Euler equations of gas dynamics, to efficiently solve two-dimensional systems of hyperbolic conservation laws on non-Cartesian domains

$$\begin{cases} u_t + \nabla \cdot f(u) = 0, \\ u(x, 0) = u_0(x). \end{cases} \tag{1.1}$$

The key idea of finite difference WENO schemes is a nonlinear combination of lower order approximations to fluxes in order to obtain a high order approximation. The choice of weights distributed to each candidate stencil, which is a nonlinear function of grid values, is crucial for the success of WENO schemes. For hyperbolic systems, WENO schemes are based on local characteristic decompositions and flux splitting in order to get better numerical solutions, but with additional computational cost. Both procedures are key elements of WENO schemes. However, the computational cost for using nonlinear weights and a local characteristic decomposition is high. It should be mentioned that when the number of equations and spatial dimension are increased, the growth of the computational cost is considerable. In [11], we only considered hybrid WENO schemes on uniform grids for Cartesian domains. It is well known that if only uniform grids are used for non-Cartesian domains, the numerical results are *unsatisfactory*. Therefore, it is desirable to develop efficient WENO schemes for non-Cartesian domains, which can keep original properties (e.g., the essentially non-oscillatory property near discontinuities and the sharp shock transition) and more importantly obtain higher computational efficiency than the original schemes. There have been a few attempts to overcome this drawback in the one-dimensional case [3, 6, 15].

To attempt to circumvent the shortcomings of WENO scheme, the hybrid point of view is noteworthy. In [11], Li and Qiu presented a hybrid version of WENO schemes with high order upwind linear schemes for Euler equations of gas dynamics. The main idea of the scheme is to identify discontinuities by a given indicator, reconstruct the numerical flux by a WENO reconstruction in discontinuous regions and by a upwind linear reconstruction in smooth regions where local characteristic decompositions and nonlinear weights for part of the procedure are avoided. Compared with other hybrid schemes in [3, 6, 15], ours is more straightforward due to the close relation between the WENO reconstruction and the upwind linear reconstruction.

As mentioned above, an important ingredient of hybrid schemes is an indicator to automatically identify the location of a discontinuity in the solution. The indicators in [11] are mainly based on the troubled cell (a cell that contains a discontinuity) indicators, also called limiters for discontinuous Galerkin (DG) finite element methods. These have been investigated by Qiu and Shu [16]. Recently, Zhu and Qiu [25] took these limiters as troubled cell indicators for adaptive Runge-Kutta discontinuous Galerkin (RKDG) methods. In [11], we used the troubled cell indicators as discontinuity indicators in order to identify discontinuities of the solution. By comparing different indicators for one-dimensional Euler equations, we choose four better indicators: a troubled cell indicator based on the average total variation of the solution

(ATV), the minmod-based TVB limiter (TVB) [2], the multi-resolution analysis of Harten (MR) [5] and the shock-detection technique by Krivodonova et al. (KXRCF) [8]. Hybrid WENO schemes with the above four discontinuity indicators result in less CPU time, smaller percentages of reconstruction of the fluxes using WENO reconstruction.

Furthermore, by virtue of the aforementioned four indicators in [11], Li et al. [10] also investigated shallow water equations with source terms due to a non-flat bottom topography and designed hybrid well-balanced WENO schemes, in which rigorous theoretical analysis as well as extensive numerical results all indicate that the resulting schemes can maintain the exact conservation property (exact C-property) [1]. This is crucial for hyperbolic balance laws [14], in particular to gain higher efficiency than the original well-balanced WENO schemes as reported in [24].

In this paper, we apply hybrid WENO schemes for two-dimensional systems of hyperbolic conservation laws on non-Cartesian domains in the hope of obtaining similar advantageous properties as those of hybrid WENO schemes in [10, 11]. Due to the page limitation, we only consider the better indicators mentioned in [11], namely ATV, TVB, MR and KXRCF.

The outline of this paper is as follows: in Section 2, we present formulations of governing equations in the framework of a general coordinate system; in Section 3, we describe the hybrid WENO scheme with high order upwind linear scheme; extensive two-dimensional numerical examples are tested to demonstrate performance of the current scheme in addressing issues of the computational efficiency (less CPU time and smaller percentages of reconstruction of the numerical fluxes using the WENO reconstruction) and the non-oscillatory property in Section 4; concluding remarks are given in Section 5.

2 Governing equations in a general coordinate system

It is important to note that high order (third and higher order) finite difference WENO schemes can be applied only to uniform or smoothly varying grids (e.g., curvilinear grids) [17, 18]. In general, when dealing with non-Cartesian domains, the most well-known approach is based on transforming non-Cartesian domains in physical spaces to Cartesian domains in computational spaces [22]. Subsequently, the mapped Cartesian domains in the computational space are discretized by uniform grids. Meanwhile, the partial differential equations (PDEs) in the physical space in terms of a Cartesian coordinate system is transformed into a computational space in a general coordinate system.

Using a coordinate transformation between a Cartesian coordinate system and a general coordinate system

$$\begin{cases} \xi = \xi(x, y) \\ \eta = \eta(x, y), \end{cases}$$

the governing equations of two-dimensional systems of hyperbolic conservation laws in the physical space in a Cartesian coordinate system (x, y)

$$U_t + F(U)_x + G(U)_y = 0, \tag{2.1}$$

can be transformed into the computational space in a general coordinate system (ξ, η) as

$$\hat{U}_t + \hat{F}_\xi + \hat{G}_\eta = 0. \tag{2.2}$$

In order to keep the resulting schemes conservative, the governing equations in the computational space using a general coordinate system must be written primarily into a conservative form as the original governing equations in the physical space. Then the conservative variable and fluxes have the following forms

$$\hat{U} = \frac{1}{J}U, \quad \hat{F} = \frac{1}{J}[\xi_x F + \xi_y G], \quad \hat{G} = \frac{1}{J}[\eta_x F + \eta_y G], \tag{2.3}$$

with

$$J = \frac{1}{\det(B)} \text{ and } B = \begin{bmatrix} x_\xi & x_\eta \\ y_\xi & y_\eta \end{bmatrix}.$$

First, we treat the governing equations in the computational space using hybrid WENO schemes with the better indicators in [11], then we recover the numerical results in the physical space using an inverse coordinate transformation.

3 Hybrid WENO schemes with high order upwind linear schemes

In this section, we present the details of the procedure for implementing hybrid schemes of WENO schemes with high order upwind linear schemes. For simplicity, we consider the above procedures in the physical space using a Cartesian coordinate system (x, y). The procedure in the computational space using a general coordinate system (ξ, η) is similar to that in the physical space.

First, we use the one-dimensional scalar hyperbolic conservation law as an example

$$\begin{cases} u_t + f(u)_x = 0, \\ u(x, 0) = u_0(x). \end{cases} \tag{3.4}$$

For simplicity, we assume that grid points $\{x_j\}$ are uniform with $\Delta x = x_{j+1} - x_j$, $x_{j+1/2} = x_j + \Delta x/2$ and denote cells by $I_j = [x_{j-1/2}, x_{j+1/2}]$, $j = 1, 2, \cdots N$. The semidiscrete conservative high order finite difference scheme for Eq. 3.4 is given by

$$\frac{du_j(t)}{dt} = -\frac{1}{\Delta x}(\hat{f}_{j+1/2} - \hat{f}_{j-1/2}), \tag{3.5}$$

where $u_j(t)$ is the numerical approximation to the point value $u(x_j, t)$, and numerical fluxes $\hat{f}_{j+1/2}$ approximate $h_{j+1/2} = h(x_{j+1/2})$ to a high order accuracy with $h(x)$ implicitly defined as in [7]

$$f(u(x)) = \frac{1}{\Delta x} \int_{x-\Delta x/2}^{x+\Delta x/2} h(\xi)d\xi. \tag{3.6}$$

Using upwinding for stability, we split a general flux into two parts either globally or locally

$$f(u) = f^+(u) + f^-(u), \tag{3.7}$$

with $df^+(u)/du \geq 0$ and $df^-(u)/du \leq 0$. For simplicity, we define

$$f^{\pm}(u) = \frac{1}{2}(f(u) \pm \alpha u), \tag{3.8}$$

where $\alpha = \max_u |f'(u)|$ and the maximum is taken over the whole relevant range of u. This is the global Lax-Friedrichs flux splitting. The numerical fluxes $\hat{f}^+_{j+1/2}$ and $\hat{f}^-_{j+1/2}$ are related to $f^+(u)$ and $f^-(u)$, respectively, and will be reconstructed using either a WENO reconstruction in the discontinuous vicinity or a high order upwind linear reconstruction in smooth regions. The details of the reconstructed numerical fluxes $\hat{f}_{j+1/2}$ will be presented in subsection (3.2). Finally, we obtain the numerical fluxes

$$\hat{f}_{j+1/2} = \hat{f}^+_{j+1/2} + \hat{f}^-_{j+1/2},$$

and the semidiscrete scheme (3.5) written as an ordinary differential equation (ODE) system

$$u_t = L(u). \tag{3.9}$$

The ODE system is discretized in time by a total variation diminishing (TVD) Runge-Kutta method [19, 20]. For example the third order Runge-Kutta method is given by

$$\begin{aligned} u^{(1)} &= u^n + \Delta t L(u^n), \\ u^{(2)} &= \frac{3}{4}u^n + \frac{1}{4}u^{(1)} + \frac{1}{4}\Delta t L(u^{(1)}), \\ u^{n+1} &= \frac{1}{3}u^n + \frac{2}{3}u^{(2)} + \frac{2}{3}\Delta t L(u^{(2)}). \end{aligned} \tag{3.10}$$

3.1 Algorithm for the hybrid WENO scheme

The procedure of $(2r+1)$-th order hybrid WENO schemes with $(2r+1)$-th order upwind linear scheme is then described as follows using a given indicator.

Step 1. The troubled cell indicator is applied to identify locations of discontinuities of the numerical solution only once, at the beginning of the Runge-Kutta time discretization procedure.

Step 2. Reconstruction of the numerical fluxes is based on either the $(2r+1)$-th order WENO reconstruction in the discontinuous vicinity or the $(2r+1)$-th order upwind linear reconstruction in the smooth vicinity. The numerical fluxes $\hat{f}^+_{j+1/2}$ and $\hat{f}^-_{j-1/2}$ will be reconstructed using WENO reconstruction in stencils which contain a troubled cell identified in Step 1. For example, let I_{j_0} be a troubled cell, then there are $(2r+1)$ stencils $\{x_{j_0-r+l}, \ldots, x_{j_0+r+l}\}$, $l = -r, \cdots, r$ which contain a discontinuity. The numerical fluxes $\hat{f}^+_{j_0+l+1/2}$ and $\hat{f}^-_{j_0+l-1/2}$, $l = -r, \cdots, r$ will be reconstructed using the $(2r+1)$-th order WENO reconstruction in these stencils. The numerical fluxes $\hat{f}^+_{j+l+1/2}$ and $\hat{f}^-_{j+l-1/2}$ will be reconstructed using the $(2r+1)$-th order upwind linear reconstruction in the stencils which do not contain any troubled cells. Finally, we obtain the numerical fluxes

$\hat{f}_{j+1/2} = \hat{f}^+_{j+1/2} + \hat{f}^-_{j+1/2}$ in Eq. 3.5. With the numerical fluxes available, we obtain the semidiscrete scheme (3.5) or (3.9) in a concise form.

Step 3.   Finally, march the next time step using a third order Runge-Kutta method (3.10).

3.2 Reconstruction of numerical fluxes

In this subsection, we present procedures for the reconstruction of the numerical fluxes $\hat{f}^+_{j+1/2}$ using the $(2r + 1)$-th order WENO reconstruction or the $(2r + 1)$-th order upwind linear reconstruction.

In the WENO reconstruction procedure, $\hat{f}^+_{j+1/2}$ is expressed as in [7]

$$\hat{f}^+_{j+1/2} = \sum_{k=0}^{r} \omega_k q_k^r \left(f^+_{j+k-r}, \ldots, f^+_{j+k} \right), \tag{3.11}$$

where ω_k are nonlinear weights, $f_i^+ = f^+(u_i)$, $i = j - r, \ldots, j + r$, and

$$q_k^r (g_0, \ldots, g_r) = \sum_{l=0}^{r} a_{k,l}^r g_l \tag{3.12}$$

is a $(r + 1)$ order approximation to $\hat{f}^+_{j+1/2}$ on the k-th stencil $S_k = (x_{j+k-r}, \ldots, x_{j+k})$, $k = 0, 1, \ldots, r$, and $a_{k,l}^r, 0 \leq k, l \leq r$, are constant coefficients, see [17] for details.

The nonlinear weights ω_k in Eq. 3.11 satisfy

$$\omega_k \geq 0 \text{ and } \sum_{k=0}^{r} \omega_k = 1,$$

and are designed to yield $(2r + 1)$-th order accuracy in regions where the solution is smooth. In [7, 17] the nonlinear weights ω_k are formulated as

$$\omega_k = \frac{\alpha_k}{\sum\limits_{l=0}^{r} \alpha_l} \text{ with } \alpha_k = \frac{C_k^r}{(\varepsilon + IS_k)^2}, \ k = 0, 1, \ldots, r, \tag{3.13}$$

where C_k^r are linear weights, see [17]. IS_k are smoothness indicators of $f^+(u)$ on stencils $S_k, k = 0, 1, \ldots, r$, and ε is a small constant used here to avoid the denominator becoming zero. We take $\varepsilon = 10^{-6}$ in all test cases in this paper. We employ the smoothness indicators proposed in [7, 17]

$$IS_k = \sum_{l=1}^{r} \int_{x_{j-1/2}}^{x_{j+1/2}} (\Delta x)^{2l-1} \left(q_k^{(l)}(x) \right)^2 dx,$$

where $q_k(x)$ is the reconstruction polynomial of $f^+(u)$ on the stencil S_k such that

$$\frac{1}{\Delta x} \int_{I_i} q_k(x) dx = f_i^+, \ i = j + k - r, \ldots, j + k,$$

and $q_k^{(l)}$ is the l-th derivative of $q_k(x)$.

For the high order upwind linear reconstruction, we use all the r candidate stencils, i.e., $S = \bigcup_{k=0}^{r} S_k$, which contains all $(2r + 1)$ grid point values of $f^+(u)$, to obtain a $(2r + 1)$-th order approximation to $\hat{f}_{j+1/2}^+$ in smooth parts such that

$$\frac{1}{\Delta x} \int_{I_i} q_r^{2r+1}(x)dx = f_i^+, \; i = j - r, \ldots, j + r,$$

and

$$\hat{f}_{j+1/2}^+ = q_r^{2r+1}\left(f_{j-r}^+, \ldots, f_{j+r}^+\right) = \sum_{l=0}^{2r} b_l f_{j+l-r}^+, \tag{3.14}$$

where b_l, $0 \leq l \leq 2r$ are constant coefficients, for details, we refer to [17]. By simple algebraic operations, we get

$$\hat{f}_{j+1/2}^+ = q_r^{2r+1}(f_{j-r}^+, \ldots, f_{j+r}^+) = \sum_{k=0}^{r} C_k^r q_k^r(f_{j+k-r}^+, \ldots, f_{j+k}^+), \tag{3.15}$$

here the coefficients C_k^r are the linear weights in Eq. 3.13, and in smooth parts $\omega_k = C_k^r + O((\Delta x)^r)$, $k = 0, 1, \ldots, r$. Thus C_k^r are called *optimal weights*.

The procedure for the reconstruction of $\hat{f}_{j+1/2}^-$ is mirror symmetric to that of $\hat{f}_{j+1/2}^+$ with respect to $x_{j+1/2}$, we will not present it here.

Remark 1 For systems, in order to achieve a higher quality approximation at the price of more complex computations, the WENO reconstruction is always applied to the local characteristic decomposition, see [17] for details, while the upwind linear reconstructions is used component by component. For the two-dimensional case, the reconstructions of the numerical fluxes are based on a dimension by dimension implementation.

3.3 Description of the troubled cell indicators

In this subsection, we briefly review the four better troubled cell indicators in [11]. The first one and the third one are based on the variation of the solution and the multi-resolution analysis [5], respectively. The remaining indicators result from the limiters of DG method [16, 25].

For convenience of presentation for the troubled cell indicators, we construct a quadratic polynomial on cell I_j at time step t_n, denoted by

$$P_2(x) = u_j^{(0)} + u_j^{(1)} \frac{x - x_j}{\Delta x} + u_j^{(2)} \left[\left(\frac{x - x_j}{\Delta x} \right)^2 - \frac{1}{12} \right], \; x \in [x_{j-1/2}, x_{j+1/2}]. \tag{3.16}$$

These are uniquely determined by the following interpolation conditions

$$P_2(x_k) = u_k^n, \; k = j - 1, \; j, \; j + 1,$$

i.e., $P_2(x)$ interpolates the data u_k^n in the sense of point values. The resulting expressions of its coefficients are

$$u_j^{(0)} = \frac{1}{24}\left(u_{j-1}^n + 22u_j^n + u_{j+1}^n\right), \quad u_j^{(1)} = \frac{1}{2}\left(u_{j+1}^n - u_{j-1}^n\right),$$

$$u_j^{(2)} = \frac{1}{2}\left(u_{j-1}^n - 2u_j^n + u_{j+1}^n\right).$$

We next describe different troubled cell indicators used in [11] in detail.

1. A troubled cell indicator based on the average total variation of the solution. (ATV, we will use the same abbreviation as in [16, 25] for each indicator). Let TV denote the total variation of the solution at the time step t_n,

$$TV \equiv TV(u^n) = \sum_j \left|u_{j+1}^n - u_j^n\right|.$$

If $\left|u_{j+1}^n - u_j^n\right| \geq \mu\frac{TV}{N}$, we declare that in the cell $[x_j, x_{j+1}]$ the solution has a discontinuity, and cells I_j and I_{j+1} are identified as troubled cells. Here N is the number of cells. $0 < \mu < 1$ is a ATV constant parameter. The choice of μ depends on the solution. It is common in the literature to look at the variation of the solution in order to indicate the presence of discontinuities at a particular location [3, 15]. Moreover this simple definition of the discontinuity guarantees that both shock waves and contact discontinuities are properly identified. However it is difficult to choose μ accurately, as μ is problem dependent. If μ is chosen too small, this will increase computational cost unnecessarily; however if μ is chosen too large, spurious oscillations will appear.

2. The minmod-based TVB limiter [2] (TVB). Let

$$\tilde{u}_j = P_2(x_{j+1/2}) - u_j^{(0)}, \quad \tilde{\tilde{u}}_j = -P_2(x_{j-1/2}) + u_j^{(0)}.$$

These are modified using the modified minmod function $\tilde{m}$, namely

$$\begin{aligned}\tilde{u}_j^{(mod)} &= \tilde{m}\left(\tilde{u}_j, u_{j+1}^{(0)} - u_j^{(0)}, u_j^{(0)} - u_{j-1}^{(0)}\right),\\ \tilde{\tilde{u}}_j^{(mod)} &= \tilde{m}\left(\tilde{\tilde{u}}_j, u_{j+1}^{(0)} - u_j^{(0)}, u_j^{(0)} - u_{j-1}^{(0)}\right),\end{aligned} \tag{3.17}$$

where $\tilde{m}$ is given by

$$\tilde{m}(a_1, a_2, \ldots, a_n) = \begin{cases} a_1 & \text{if } |a_1| \leq M(\Delta x)^2, \\ m(a_1, a_2, \ldots, a_n) & \text{otherwise,} \end{cases} \tag{3.18}$$

and the original minmod function m is defined as

$$m(a_1, a_2, \ldots, a_n) = \begin{cases} s \cdot \min_{1 \leq j \leq n} |a_j| & \text{if } sign(a_1) = sign(a_2) = \cdots = sign(a_n) = s, \\ 0 & \text{otherwise.} \end{cases} \tag{3.19}$$

The TVB limiter parameter $M > 0$ is a constant.

If $\tilde{u}_j^{(mod)} \neq \tilde{u}_j$ or $\tilde{\tilde{u}}_j^{(mod)} \neq \tilde{\tilde{u}}_j$, we declare the cell I_j as a troubled cell. Unfortunately, the TVB limiter parameter M also depends on the equation under consideration. There is no automatic switch that works well for all situations. For scalar problems it is possible to estimate M by the initial condition as in [2]

(M is proportional to the second derivative of the initial data at smooth extrema), however it is difficult to estimate M for system of equations. If M is chosen too small, more cells containing discontinuities will be identified than necessary, which increases computational cost; however if M is chosen too large, spurious oscillations will arise.

3. The multi-resolution analysis of Harten [5] (MR). This relies on given point values u_j of the solution $u(x)$. Let $\tilde{u}_j$ denote the approximation to u_j which is obtained from the unique polynomial $\tilde{u}(x)$ of degree one that interpolates $u(x)$ at x_{j-1} and x_{j+1},

$$\tilde{u}_j = \tilde{u}(x_j) = \frac{1}{2}(u_{j-1} + u_{j+1}),$$

and let d_j denote the corresponding approximation error:

$$d_j = u_j - \tilde{u}_j.$$

If $u(x)$ at $x = \bar{x}$ has $p - 1$ continuous derivatives and a jump discontinuity in its p-th derivative as denoted by $[\cdot]$, then for x_j near $\bar{x}$

$$d_j \approx \begin{cases} (\Delta x)^p [u^{(p)}] & p \le 2 \\ (\Delta x)^2 u^{(2)} & p \ge 2. \end{cases} \tag{3.20}$$

In this paper, if $|d_j| \ge \varepsilon_{MR} \Delta x$, the cell I_j is identified as a troubled cell, here ε_{MR} is a multi-resolution parameter.

4. The shock-detection technique by Krivodonova et al. [8] (KXRCF). Partition the boundary of a cell I_j into two portions ∂I_j^- and ∂I_j^+, where the flow is into ($\vec{v} \cdot \vec{n} < 0$, $\vec{n}$ is the normal vector to ∂I_j) and out of ($\vec{v} \cdot \vec{n} > 0$) I_j, respectively. The cell I_j is identified as a troubled cell, when

$$\frac{\left| \int_{\partial I_j^-} (u^h|_{I_j} - u^h|_{I_{n_j}}) ds \right|}{h_j^{\frac{k+1}{2}} |\partial I_j^-| \| u^h|_{I_j} \|} > 1, \tag{3.21}$$

here h_j is the radius of the circumscribed circle in the element I_j. I_{n_j} is the neighbor of I_j on the side of ∂I_j^- and the norm is based on an element average for the one-dimensional case. Herein, we take k as the degree of the polynomial $P_2(x)$ in Eq. 3.16, namely $k = 2$.

Remark 2 From the above list of indicators, we observe that ATV, TVB and MR indicators are all dependent on parameters, while the KXRCF indicator is free of parameters. The parameter-free indicator is desirable for general hyperbolic conservation laws. For two-dimensional Euler equations of gas dynamics, we take the entropy in the computational space as an indicator variable to identify troubled cells. For shallow water equations, we apply both the water depth and the water velocity simultaneously in the computational space to detect troubled cells. The troubled cell indicators work in ξ- and η-direction, respectively, to identify troubled cells.

Remark 3 All the indicators except ATV depend only on the cell and its two neighboring cells, so the reconstruction of the numerical flux is dependent on the cell and

its $2r$ neighboring cells, these local properties guarantee that this hybrid approach is a highly parallel method.

Remark 4 This technique in this paper can be applied to finite volume WENO schemes directly and the implementation of the indicators is nearly the same. The main difference between the two types of schemes lies in the reconstruction procedure. For the finite difference scheme, we obtain the numerical fluxes using a WENO or upwind linear reconstruction directly; while for the finite volume scheme, we get $u^{\pm}_{j+1/2}$ first, which ultimately results in the numerical fluxes.

4 Numerical results

This section is devoted to extensive numerical experiments for two-dimensional systems of hyperbolic conservation laws. This includes the Euler equations and shallow water equations in order to demonstrate the performance of the current hybrid WENO scheme. Comparisons are concentrated mainly on using CPU time and percentages of the reconstruction of the fluxes using WENO reconstruction. In all the numerical examples, we take the ATV parameter μ as 0.6. The TVB parameter M and the multi-resolution parameter ε_{MR} are chosen to be 0.01, 0.05 and 1., 0.8 for Euler equations and shallow water equations, respectively. In all test cases, we adopt the third order Runge-Kutta method for the time discretization, and the CFL number is taken as 0.6. In the figures for the numerical results, the solid line stands for reference solutions and "□" represents numerical solutions. In time history figures, each symbol "○" denotes the position of the reconstruction of the flux using WENO reconstruction.

4.1 Euler equations of the gas dynamics

First, we consider two-dimensional Euler equations using the present hybrid WENO scheme. The PDE for the two-dimensional Euler equations in the physical space in Cartesian coordinate system (x, y) is as follows

$$
\begin{bmatrix} \rho \\ \rho u \\ \rho v \\ E \end{bmatrix}_t + \begin{bmatrix} \rho u \\ \rho u^2 + p \\ \rho u v \\ u(E + p) \end{bmatrix}_x + \begin{bmatrix} \rho v \\ \rho u v \\ \rho v^2 + p \\ v(E + p) \end{bmatrix}_y = 0, \qquad (4.22)
$$

where ρ is the density, u and v are the velocities in $x-$ and $y-$direction, respectively, E is the total energy, and p is the pressure, which is related to the total energy by $E = \frac{p}{\gamma - 1} + \frac{1}{2}\rho(u^2 + v^2)$ with $\gamma = 1.4$.

Example 4.1 Cylindrical explosion problem [23]. This test case is similar to a two-dimensional Riemann problem. Flow variables take constant values in each of these

regions and are joined by a circular discontinuity initially. The two constant states are chosen to be

$$(\rho, u, v, p) = \begin{cases} (1, 0, 0, 1) & \text{if } x^2 + y^2 \le 0.4^2 \\ (0.125, 0, 0, 0.1) & \text{otherwise.} \end{cases}$$

The physical domain is a circular domain with radius $r = 1$ positioned at the origin in the $x - y$ plane. We choose the computational domain to be $[0, 1] \times [0, 2\pi]$ in the $r - \theta$ plane. The transformation between Cartesian coordinate system (x, y) and a general coordinate system (r, θ) is given by

$$\begin{cases} x = r \cos(\theta) \\ y = r \sin(\theta). \end{cases} \tag{4.23}$$

See [21] for the governing equations and the explicit presentation of eigenvalues and eigenvectors of the two-dimensional Euler equations with a general coordinate system. We solve the test case up to $t = 0.25$.

In Table 1, we document CPU time and percentages of the reconstruction of the fluxes using WENO reconstruction for the third and fifth order schemes, respectively. We can see that the hybrid WENO scheme costs about one third of the CPU time of the pure WENO scheme. We clearly see that these are smaller percentages for the reconstruction of the fluxes using WENO reconstruction with finer grids, as we expect.

Table 1 Cylindrical explosion problem

$N_r \times N_\theta$	Scheme or indicators	Third order scheme		Fifth order scheme	
		CPU	Percent	CPU	Percent
20×120	WENO	22.91	100.00	25.86	100.00
	ATV	10.03	30.36	12.06	33.42
	TVB	11.14	32.34	13.00	37.23
	MR	12.28	41.41	13.78	43.24
	KXRCF	11.08	30.72	13.31	36.57
60×360	WENO	1704.45	100.00	1960.50	100.00
	ATV	559.45	15.97	640.19	18.30
	TVB	585.11	16.02	669.53	18.18
	MR	632.25	21.47	733.59	23.59
	KXRCF	605.75	17.39	733.47	20.66
180×1080	WENO	117048.56	100.00	119882.40	100.00
	ATV	39106.48	9.46	39256.80	10.36
	TVB	35646.77	6.35	36071.95	8.10
	MR	36911.52	8.31	38266.00	9.39
	KXRCF	40584.63	9.05	42582.03	10.00

Comparison of CPU time and percentages of the reconstruction of the fluxes using WENO reconstruction between pure WENO and hybrid WENO schemes
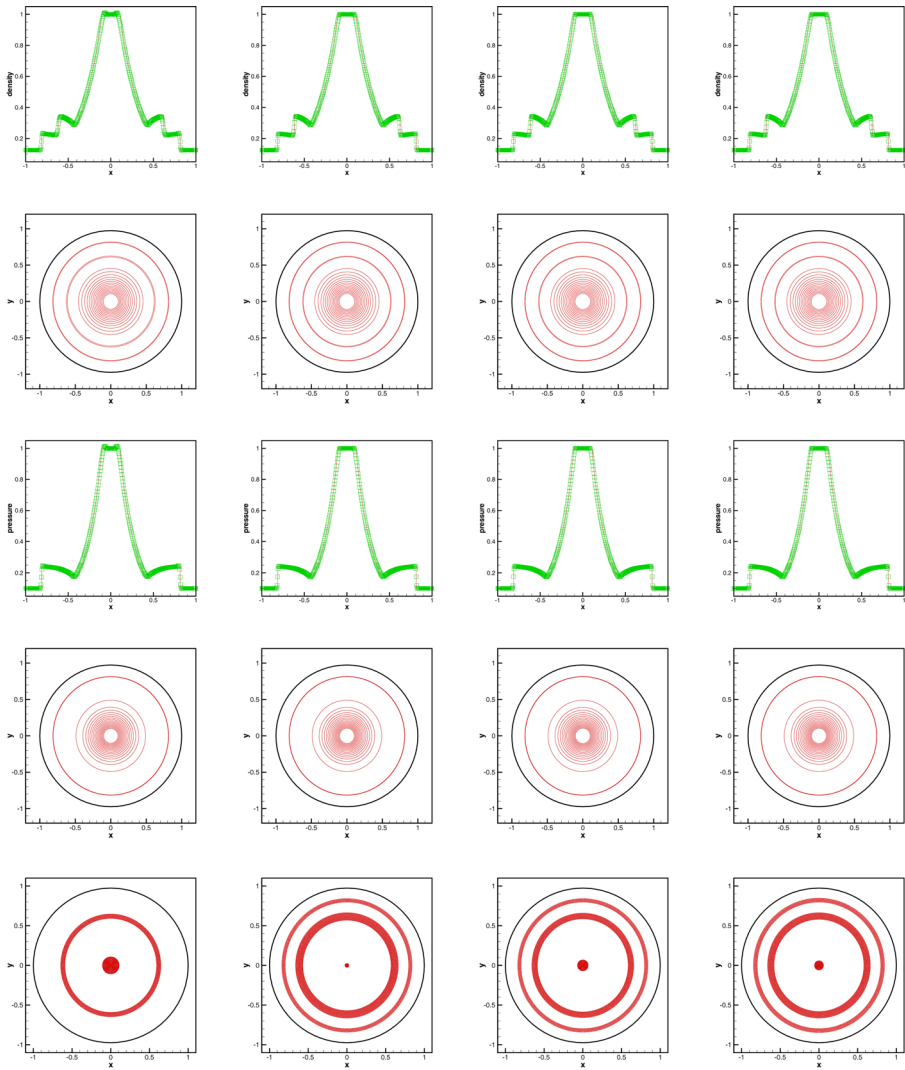
Fig. 1 Cylindrical explosion problem using a fifth order scheme with $180 \times 1080 (r \times \theta)$ cells, $t = 0.25$. From *top* to *bottom*: 1D cut of density for the $y = 0$ plane, density contours, 1D cut of pressure for the $y = 0$ plane, pressure contours and the cells in which fluxes are reconstructed using WENO reconstruction for the last time step. From *left* to *right*: ATV, TVB, MR and KXRCF

Due to the cylindrical symmetry, the solutions of the full two-dimensional system (4.22) are equivalent to the solutions of the following cylindrical one-dimensional system with geometric source terms [23]

$$
\begin{bmatrix} \rho \\ \rho u \\ E \end{bmatrix}_t + \begin{bmatrix} \rho u \\ \rho u^2 + p \\ u(E + p) \end{bmatrix}_r = -\frac{1}{r} \begin{bmatrix} \rho u \\ \rho u^2 \\ u(E + p) \end{bmatrix},
\tag{4.24}
$$

with r being a radial direction, which is also solved on a very fine grid with $N = 3240$ cells as radial reference solutions to compare the numerical results. To save space, we only show the numerical results on the most refined grid with 180×1080 uniform cells using a fifth order scheme in Fig. 1. From the figures, we can clearly observe that all numerical results are axially symmetric due to the symmetry of the curvilinear grid and are in good agreement with the reference solutions. The cells where fluxes are reconstructed using WENO reconstruction at the last time step are also presented in Fig. 1.

In addition, we also compute the L^1 and L^2 errors for the density and the pressure from $x = 0$ to $x = 1$ in the $y = 0$ plane, see Tables 2 and 3, respectively. The tables imply that the hybrid WENO scheme has a slight advantage over the pure WENO scheme in terms of the accuracy of the numerical solution. We conjecture that this by product of hybrid WENO schemes thanks to the following two possible reasons: on one hand it has to do with the computation of nonlinear weights and local characteristic decompositions, which results in accumulation of truncation errors; on the other hand, it relates to the fact that limited numerical fluxes are always less accurate than unlimited ones. Herein, the WENO reconstruction is limited due to nonlinear weights, while the upwind linear reconstruction is unlimited.

Example 4.2 Flow past a semi-cylinder [4, 7]. In this test, we implement a simulation of a Mach 3 supersonic flow past a semi-cylinder. In physical space, a

Table 2 Cylindrical explosion problem

$N_r \times N_\theta$	Scheme or indicators	Third order scheme		Fifth order scheme	
		L^1 error	L^2 error	L^1 error	L^2 error
20×120	WENO	4.9496E-2	7.3251E-2	3.1897E-2	4.4988E-2
	ATV	4.7997E-2	7.1617E-2	3.1872E-2	4.4835E-2
	TVB	4.7211E-2	6.8881E-2	3.1860E-2	4.4612E-2
	MR	4.7536E-2	7.3133E-2	3.1856E-2	4.4654E-2
	KXRCF	4.6469E-2	6.7966E-2	3.1841E-2	4.4621E-2
60×360	WENO	1.8300E-2	2.9850E-2	1.0948E-2	1.8784E-2
	ATV	1.6775E-2	2.7141E-2	1.0807E-2	1.8368E-2
	TVB	1.6828E-2	2.5227E-2	1.0438E-2	1.8419E-2
	MR	1.7507E-2	2.7512E-2	1.0498E-2	1.8442E-2
	KXRCF	1.6678E-2	2.5965E-2	1.0437E-2	1.8298E-2
180×1080	WENO	5.7934E-3	1.3021E-3	3.9104E-3	9.9739E-3
	ATV	5.5396E-3	1.2130E-2	3.8376E-3	9.8447E-3
	TVB	5.4854E-3	1.2103E-2	3.8224E-3	9.9527E-3
	MR	5.5852E-3	1.2120E-3	3.8014E-3	9.9016E-3
	KXRCF	5.6833E-3	1.2292E-2	3.8067E-3	9.9426E-3

Comparison of L^1 and L^2 errors for the density between pure WENO and hybrid WENO schemes

Table 3 Cylindrical explosion problem

$N_r \times N_\theta$	Scheme or indicators	Third order scheme		Fifth order scheme	
		L^1 error	L^2 error	L^1 error	L^2 error
20×120	WENO	5.6316E-2	9.5166E-2	3.3843E-2	5.5846E-2
	ATV	5.3735E-2	9.3204E-2	3.3655E-2	5.5668E-2
	TVB	5.2504E-2	8.8971E-2	3.3545E-2	5.5668E-2
	MR	5.6180E-2	9.4940E-2	3.3621E-2	5.5747E-2
	KXRCF	5.3843E-2	9.2019E-2	3.3516E-2	5.5515E-2
60×360	WENO	1.8749E-2	3.6925E-2	1.0342E-2	2.1578E-2
	ATV	1.6846E-2	3.3085E-2	1.0468E-2	2.0921E-2
	TVB	1.6086E-2	2.9661E-2	9.9200E-3	2.0925E-2
	MR	1.7707E-2	3.3448E-2	9.9886E-3	2.0954E-2
	KXRCF	1.6552E-2	3.0831E-2	9.9007E-3	2.0698E-2
180×1080	WENO	5.0490E-3	1.2105E-2	3.5091E-3	9.3013E-3
	ATV	4.8683E-3	1.1657E-2	3.4590E-3	9.0404E-3
	TVB	5.0227E-3	1.2102E-2	3.4218E-3	9.2856E-3
	MR	4.9268E-3	1.1705E-2	3.3825E-3	9.1647E-3
	KXRCF	5.0219E-3	1.2075E-2	3.4010E-3	9.2635E-3

Comparison of L^1 and L^2 errors for the pressure between pure WENO and hybrid WENO schemes

semi-cylinder with unit radius is positioned at the origin on the $x - y$ plane. The computational domain is a rectangle $[1, 5] \times \left[\frac{\pi}{2}, \frac{3\pi}{2} \right]$ in the $r - \theta$ plane. The coordinate transformation is the same as in Eq. 4.23.

This problem is initialized by a Mach 3 flow moving from left toward the semi-cylinder. A reflective boundary condition is imposed at the surface of the cylinder, i.e., $r = 1$, an inflow boundary condition is applied at $r = 5$, and an outflow boundary condition is applied at $\theta = \frac{\pi}{2}$ and $\theta = \frac{3\pi}{2}$.

In Table 4, we make a comparison for CPU time and percentages of the reconstruction of the fluxes using WENO reconstruction for the third and fifth order schemes. We can see that the hybrid WENO scheme costs about one third to one half of the CPU time of the pure WENO scheme. We also see that the percentages of the reconstruction of the fluxes using WENO reconstruction for hybrid WENO schemes is less than 20% for both third and fifth order schemes, and smaller percentages of the reconstruction of the fluxes using WENO reconstruction with the refinement of grids as we expect. In order to save space, we only present the numerical results for the most refined grid with 320×240 uniform cells using fifth order schemes in Figs. 2 and 3. In Fig. 4, we also show the cells where the fluxes are reconstructed using WENO reconstruction at the last time step.

Table 4 Flow past a semi-cylinder

$N_r \times N_\theta$	Scheme or indicators	Third order scheme		Fifth order scheme	
		CPU	Percent	CPU	Percent
80×60	WENO	3.01	100.00	3.53	100.00
	ATV	1.38	17.57	1.31	19.20
	TVB	1.13	6.79	1.09	8.27
	MR	1.16	12.22	1.11	15.54
	KXRCF	1.18	7.09	1.15	7.75
160×120	WENO	23.98	100.00	27.85	100.00
	ATV	10.22	13.29	10.10	15.92
	TVB	8.81	4.54	7.88	5.87
	MR	9.15	10.56	8.76	14.79
	KXRCF	9.35	4.69	7.65	5.66
320×240	WENO	192.95	100.00	230.56	100.00
	ATV	82.90	11.62	81.20	12.44
	TVB	68.09	2.98	75.65	3.55
	MR	75.17	8.50	71.17	12.56
	KXRCF	69.10	2.55	78.90	3.15

Comparison of CPU time and percentages of the reconstruction of the fluxes using WENO reconstruction between pure WENO and hybrid WENO schemes
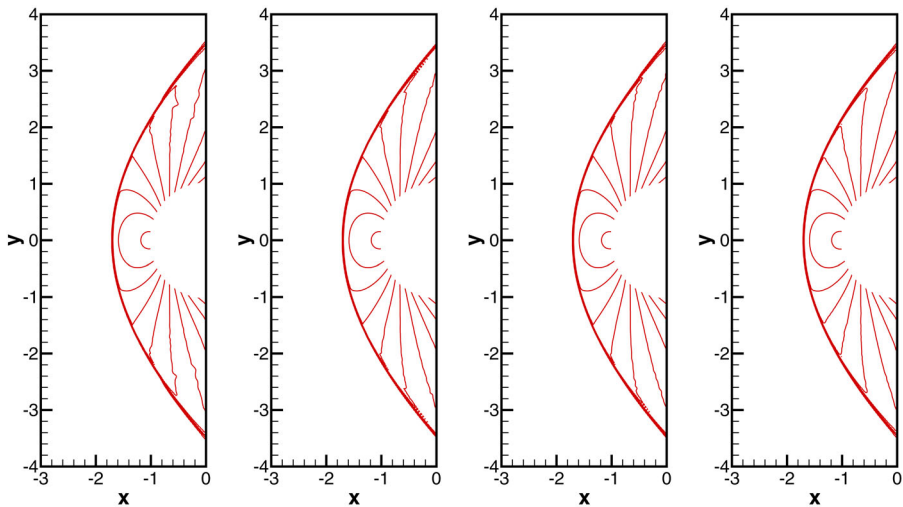

Fig. 2 Flow past a semi-cylinder using a fifth order scheme with 320×240 ($r \times \theta$) cells. Pressure contours. From *left* to *right*: ATV, TVB, MR and KXRCF
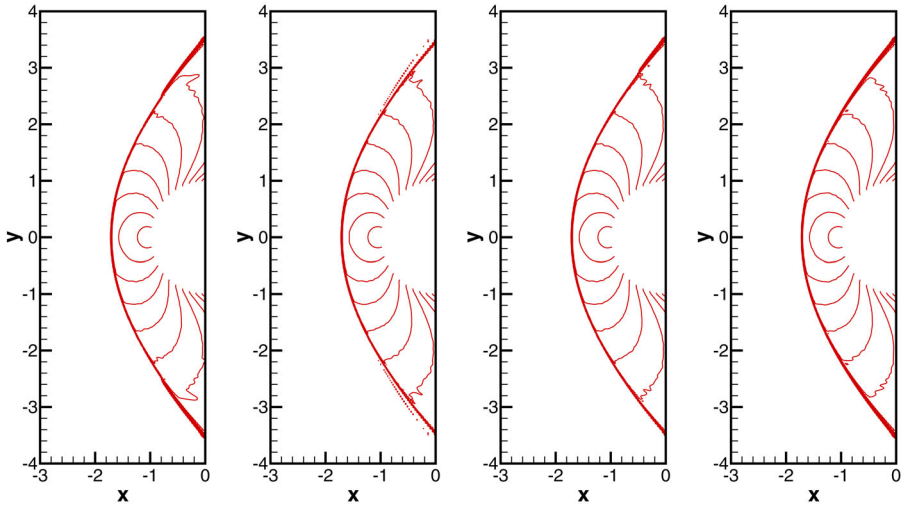
Fig. 3 Flow past a semi-cylinder using a fifth order scheme with 320×240 ($r \times \theta$) cells. Mach number contours. From *left* to *right*: ATV, TVB, MR and KXRCF

Example 4.3 Flow past a cylinder [13]. In this test, we aim to carry out a simulation of a Mach 3 supersonic flow past a full cylinder. In the physical space, a full cylinder of unit radius is positioned at the origin in the *x-y* plane. The computational domain is chosen to be $[1, 5] \times [0, 2\pi]$ in the $r - \theta$ plane. The coordinate transformation is the same as in Eq. 4.23.
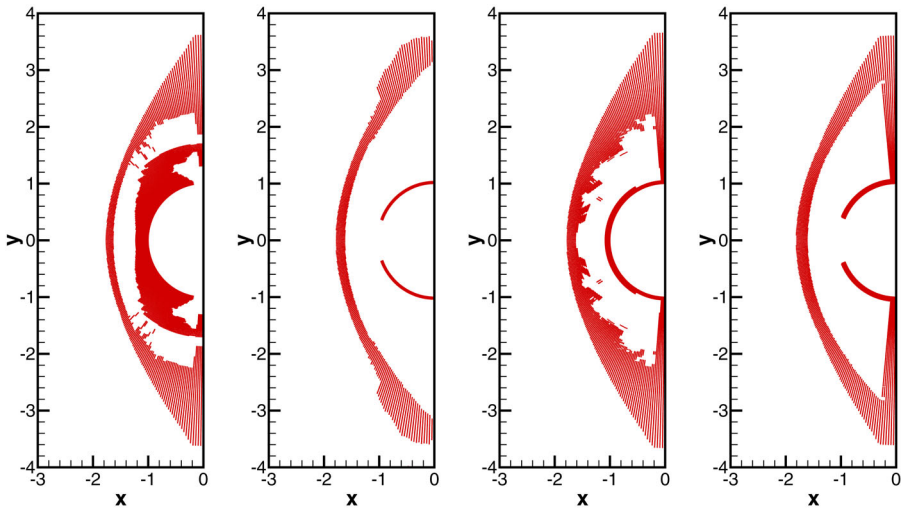

Fig. 4 Flow past a semi-cylinder using a fifth order scheme with 320×240 ($r \times \theta$) cells. The cells where the fluxes are reconstructed using WENO reconstruction at the last time step. From *left* to *right*: ATV, TVB, MR and KXRCF

Table 5 Flow past a cylinder

$N_r \times N_\theta$	Scheme or indicators	Third order scheme		Fifth order scheme	
		CPU	Percent	CPU	Percent
120×40	WENO	25.07	100.00	79.05	100.00
	ATV	13.77	25.14	40.99	27.53
	TVB	16.80	24.55	44.27	30.86
	MR	15.68	31.36	42.51	33.05
	KXRCF	17.66	26.79	49.85	30.91
240×80	WENO	239.08	100.00	635.76	100.00
	ATV	108.62	19.77	316.09	20.11
	TVB	123.96	18.02	335.90	22.46
	MR	117.40	24.74	329.49	26.05
	KXRCF	128.53	17.93	343.82	22.28
480×160	WENO	2134.96	100.00	4294.57	100.00
	ATV	842.33	11.71	2256.12	13.84
	TVB	974.43	16.53	2489.08	18.47
	MR	928.28	18.41	2373.81	20.87
	KXRCF	988.86	17.06	2468.76	18.71

Comparison of CPU time and percentages of the reconstruction of the fluxes using WENO reconstruction between pure WENO and hybrid WENO schemes

This problem is initialized by a Mach 3 flow moving from left toward a cylinder. A reflective boundary condition is imposed at the surface of the cylinder, i.e., $r = 1$.

The comparison of CPU time and percentages of reconstruction of the fluxes using WENO reconstruction for the pure and hybrid WENO schemes is documented in Table 5. We can see that the hybrid WENO scheme costs about half of the CPU time of the pure WENO scheme for third and fifth order schemes, respectively. We also see that the percentages of the reconstruction of the fluxes using WENO reconstruction
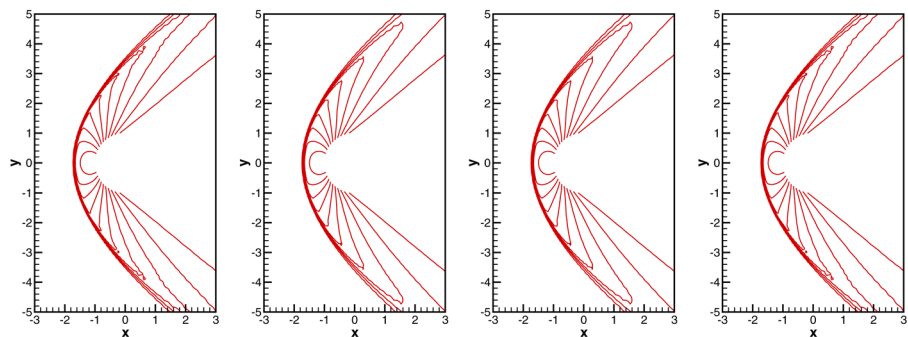

Fig. 5 Flow past a cylinder using a fifth order scheme with $480 \times 160(r \times \theta)$ cells. Pressure contours. From *left* to *right*: ATV, TVB, MR and KXRCF
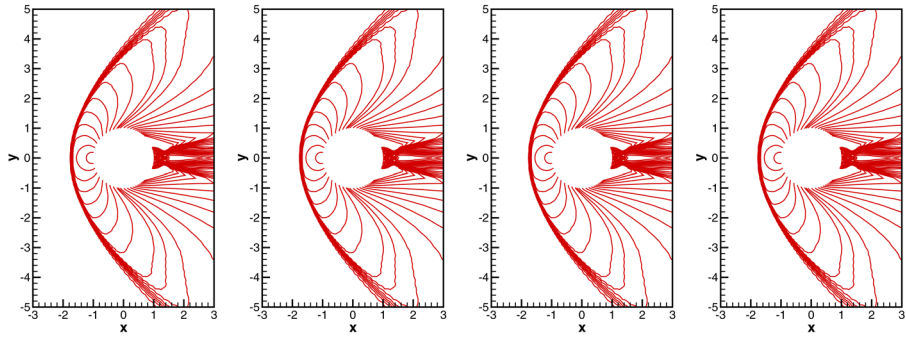
Fig. 6 Flow past a cylinder using a fifth order scheme with $480 \times 160(r \times \theta)$ cells. Mach number contours. From *left* to *right*: ATV, TVB, MR and KXRCF

for the hybrid WENO scheme is less than 35 % for both third and fifth order schemes. Smaller percentages of the reconstruction of the fluxes using WENO reconstruction on finer grids, as we expect. To save space, we only show the numerical results on the most refined grid with 480×160 uniform cells by fifth order schemes in Figs. 5 and 6. The cells where the fluxes are reconstructed using WENO reconstruction at the last time step are presented in Fig. 7.

4.2 Shallow water equations

Lastly, we solve shallow water equations using the current hybrid WENO scheme. The PDE for the two-dimensional case in a Cartesian coordinate system has the following form

$$\begin{bmatrix} h \\ hu \\ hv \end{bmatrix}_t + \begin{bmatrix} hu \\ hu^2 + \frac{1}{2}gh^2 \\ huv \end{bmatrix}_x + \begin{bmatrix} hv \\ hvu \\ hv^2 + \frac{1}{2}gh^2 \end{bmatrix}_y = 0. \qquad (4.25)$$
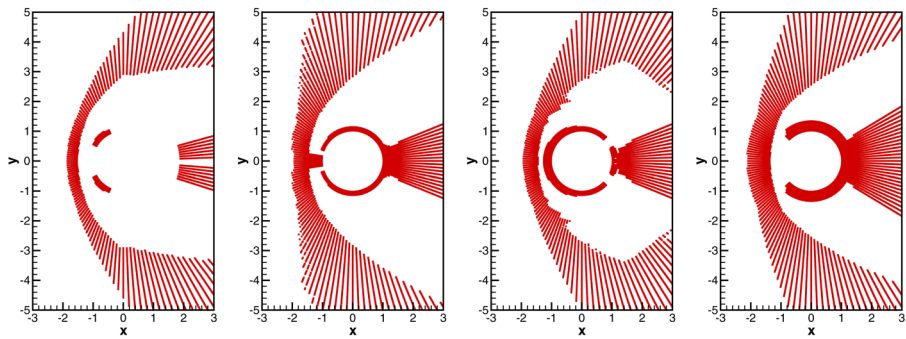

Fig. 7 Flow past a cylinder using a fifth order scheme with $480 \times 160(r \times \theta)$ cells. The cells where the fluxes are reconstructed using WENO reconstruction at the last time step. From *left* to *right*: ATV, TVB, MR and KXRCF

Here h stands for the water depth, u and v are the water velocity in the x- and y-directions, respectively, and g denotes the gravitational constant, which is taken as 9.812.

Example 4.4 Circular dam-break problem. Here we consider an idealized circular dam-break problem [22]. We assume a dam to be enclosed by an infinitely thin circular wall with radius $r = 2.5$ in a circular physical domain with radius $r = 20$ in the $x - y$ plane. The initial conditions are given by

$$h(x, y, 0) = \begin{cases} 2.5 \text{ if } x^2 + y^2 \leq 2.5^2 \\ 0.5 \text{ otherwise,} \end{cases} \text{ and } u(x, y, 0) = v(x, y, 0) = 0.$$

The dam wall is assumed to collapse instantaneously.

The flow becomes rapidly trans-critical due to the difference in the water depth. We implement this simulation on a curvilinear grid and study the wave propagation phenomena. Since this is an axially symmetric flow, we choose the computational domain to be in the $r - \theta$ plane. The coordinate transformation is defined as in Eq. 4.23. We refer to Appendix A for the explicit representations of the eigenvalues and eigenvectors for the two-dimensional shallow water equations in a general coordinate system. We solve this test case up to $t = 0.4$.

In Table 6, we document the CPU time and percentages of the reconstruction of the fluxes using WENO reconstruction for the third and fifth order schemes. We clearly

Table 6 Circular dam-break problem

$N_r \times N_\theta$	Scheme or indicators	Third order scheme		Fifth order scheme	
		CPU	Percent	CPU	Percent
60×20	WENO	1.42	100.00	1.66	100.00
	ATV	0.50	25.87	0.53	22.66
	TVB	0.39	8.98	0.44	11.06
	MR	0.44	11.43	0.47	14.37
	KXRCF	0.47	10.33	0.55	14.38
180×60	WENO	99.30	100.00	115.75	100.00
	ATV	32.44	15.57	32.52	15.02
	TVB	29.61	6.01	28.03	6.92
	MR	31.00	10.53	29.42	10.71
	KXRCF	31.75	6.57	31.25	8.04
540×180	WENO	6078.10	100.00	8848.41	100.00
	ATV	2263.56	12.50	2347.80	12.43
	TVB	1977.13	3.46	2059.61	3.47
	MR	2028.36	8.05	2054.34	7.24
	KXRCF	2148.83	3.20	2203.48	3.28

Comparison of CPU time and percentages of the reconstruction of the fluxes using WENO reconstruction between pure WENO and hybrid WENO schemes
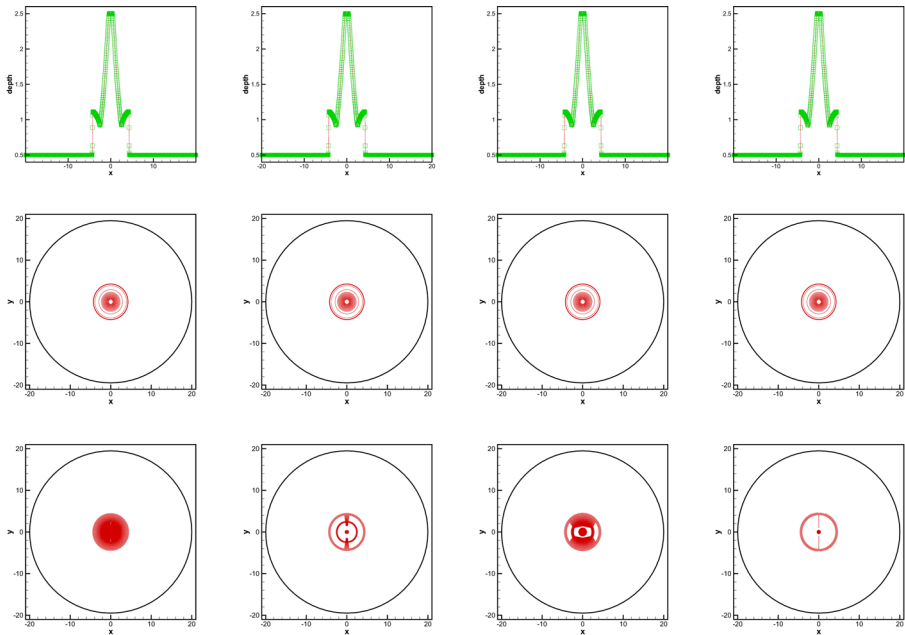
Fig. 8 Circular dam-break problem using a fifth order scheme with 540×180 ($r \times \theta$) cells, $t = 0.4$. From *top* to *bottom*: 1D cut of water depth for the $y = 0$ plane, contours of the water depth and the cells where the fluxes are reconstructed using WENO reconstruction at the last time step. From *left* to *right*: ATV, TVB, MR and KXRCF

find that the hybrid WENO scheme can save about 65-70 % of the computational cost compared to the pure WENO scheme and only 26 % fewer flux reconstructions using WENO reconstruction. It is obvious that smaller percentages of the fluxes are reconstructed using WENO reconstruction on finer grids, as we expect.

As the problem has cylindrical symmetry, along the radial direction r we can derive an inhomogeneous one-dimensional system [22], namely

$$\begin{bmatrix} h \\ hu \end{bmatrix}_t + \begin{bmatrix} hu \\ hu^2 + \frac{1}{2}gh^2 \end{bmatrix}_r = -\frac{1}{r}\begin{bmatrix} hu \\ hu^2 \end{bmatrix}. \tag{4.26}$$

In order to cross-check the numerical results, we also implement numerical computations on an inhomogeneous one-dimensional system (4.26), and compare results with those obtained from two-dimensional system (4.25). This means that we solve the inhomogeneous system (4.26) on a very fine grid with $N = 3240$ cells to produce a radial reference solution. To save space, we only show the numerical results on the most refined grid with 540×180 uniform cells using a fifth order scheme and the cells where the fluxes are reconstructed using WENO reconstruction at the last time step are shown in Fig. 8. The numerical solutions agree with the reference solution well. We can clearly observe that all the numerical results are axially symmetric owning to symmetry of the curvilinear grid.

Table 7 Circular dam-break problem

$N_r \times N_\theta$	Scheme or indicators	Third order scheme		Fifth order scheme	
		L^1 error	L^2 error	L^1 error	L^2 error
60×20	WENO	0.9966	0.5370	0.6107	0.3348
	ATV	0.9898	0.5260	0.5902	0.3246
	TVB	0.9362	0.5001	0.5832	0.3204
	MR	0.9677	0.5137	0.5837	0.3205
	KXRCF	0.7625	0.4262	0.5887	0.3227
180×60	WENO	0.3388	0.2139	0.2143	0.1459
	ATV	0.3203	0.2053	0.2042	0.1427
	TVB	0.3241	0.2038	0.2034	0.1426
	MR	0.3228	0.2074	0.2040	0.1428
	KXRCF	0.2695	0.1819	0.2018	0.1418
540×180	WENO	0.1303	0.1139	0.0736	0.0727
	ATV	0.1221	0.1040	0.0670	0.0678
	TVB	0.1163	0.0999	0.0665	0.0675
	MR	0.1222	0.1040	0.0673	0.0680
	KXRCF	0.1148	0.9891	0.0674	0.0680

Comparison of L^1 and L^2 errors for the water depth between pure WENO and hybrid WENO schemes

Analogously, we compute the L^1 and L^2 errors for the water depth from $x = 0$ to $x = 20$ in the $y = 0$ plane, see Table 7. The numerical results in the table imply that the hybrid WENO scheme can also produce slightly more accurate numerical solutions compared to those of the pure WENO scheme.

Example 4.5 Fluid-structure interaction problem [9]. We consider a planar shock wave moving towards a cylinder. The initial conditions are as follows

$$(h, u, v) = \begin{cases} \left(4, \sqrt{\dfrac{45g}{8}}, 0\right) & \text{if } x \le -2 \\ (1, 0, 0) & \text{otherwise}, \end{cases}$$

here g is the gravitational constant. A bow shock will form upstream from the cylinder once the flowing water hits the cylinder. We solve this problem on the curvilinear grid in the $r - \theta$ plane. The coordinate transformation is again the same as in Eq. 4.23. We solve this test case up to $t = 0.35$.

In Table 8, we compare the CPU time and percentages of reconstruction of the fluxes using WENO reconstruction for third and fifth order schemes. We can clearly see that the hybrid WENO scheme can save about 65 % of the computational cost compared with the pure WENO scheme and almost less than 40 % of the fluxes are reconstructed using WENO reconstruction. It is obvious that a smaller percentage of the fluxes are reconstructed using WENO reconstruction with finer grids, as

Table 8 Fluid-structure interaction problem

$N_r \times N_\theta$	Scheme or indicators	Third order scheme		Fifth order scheme	
		CPU	Percent	CPU	Percent
120×40	WENO	1.03	100.00	1.26	100.00
	ATV	0.80	34.74	1.02	38.33
	TVB	0.58	35.95	0.70	39.34
	MR	0.52	33.52	0.64	37.98
	KXRCF	0.41	10.22	0.52	20.13
240×80	WENO	8.34	100.00	10.21	100.00
	ATV	3.45	30.25	4.09	32.11
	TVB	3.84	24.00	4.52	26.35
	MR	3.39	20.87	4.04	23.63
	KXRCF	3.20	10.34	3.89	13.58
480×160	WENO	70.95	100.00	85.95	100.00
	ATV	27.77	13.58	31.35	15.37
	TVB	32.53	17.12	36.28	18.70
	MR	28.78	13.71	32.56	15.84
	KXRCF	28.07	6.76	33.06	8.33

Comparison of CPU time and percentages of the reconstruction of the fluxes using WENO reconstruction between pure WENO and hybrid WENO schemes

we expect. In order to save space, we only show the numerical results on the most refined grid with 480×160 uniform cells using a fifth order scheme and the cells where the fluxes are reconstructed using WENO reconstruction at the last time step in Fig. 9.

Remark 5 Herein, we only consider the two-dimensional shallow water equations on a plane physical domain. In fact, the numerical schemes for global shallow water equations on a sphere have significant applications in the atmospheric modeling. Therein, the physical domain is on a spherical surface. Therefore, we must find a transformation that maps the non-Cartesian physical domain onto a Cartesian computational domain. The cubed sphere geometry is a desirable choice. Detailed information can be found in [12]. A cube with identical side length is inscribed into a sphere, such that eight vertices of the cube exactly touch the sphere. A central projection projects the faces of the inscribed cube onto the spherical surface. Then the sphere is decomposed into six identical regions. Based on the projection, the cube face is free of singularities and employs identical metric terms, thus resulting in a curvilinear coordinate system on the spherical surface. Eventually, we obtain a transformation between a local Cartesian coordinate system for the computational domain and a curvilinear coordinate system for the physical domain. In other words, we transform the curvilinear grid for the physical domain into the uniform Cartesian grid for
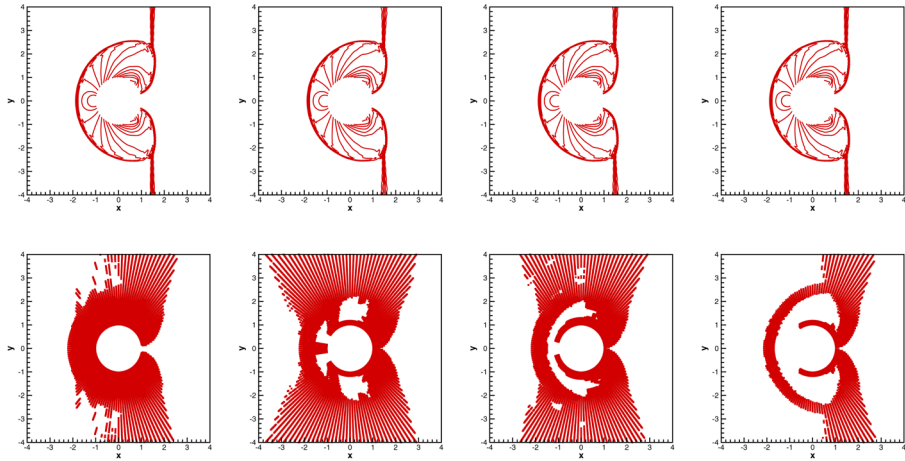
Fig. 9 Fluid-structure interaction problem using a fifth order scheme with 480×160 ($r \times \theta$) cells, $t = 0.35$. Contours of the water depth (*top*) and the cells where the fluxes are reconstructed using WENO reconstruction at the last time step (*bottom*). From *left* to *right*: ATV, TVB, MR and KXRCF

the computational domain. By means of the transformation, the generalization of the hybrid WENO scheme on the curvilinear grid is straightforward.

5 Concluding remarks

In this paper, we study hybrid WENO schemes with different indicators on curvilinear grids for non-Cartesian physical domains. A variety of benchmark examples for two-dimensional systems of hyperbolic conservation laws (including Euler equations and shallow water equations) are tested. Extensive numerical results strongly indicate that the current hybrid WENO schemes maintain the advantageous properties of the pure WENO schemes such as the non-oscillatory property near discontinuities and keeping the sharp shock transition. On the other hand, the hybrid WENO scheme has a great advantage over the pure WENO scheme in terms of improved computational efficiency. Also, the hybrid WENO scheme can result in slightly more accurate numerical solutions than the pure WENO scheme. In addition, it is observed that the KXRCF indicator is superior to other indicators since it is free of parameters. The resulting hybrid WENO scheme with the KXRCF indicator has great potential in practical applications. Our ongoing research work includes proposing a hybrid finite difference WENO scheme for the global shallow water equations on a sphere and studying the hybrid finite volume WENO scheme for unstructured grids.

Appendix A: Two-dimensional shallow water equations in a general coordinate system

Notations:

$$h \; : \; \text{water depth}$$
$$u \; : \; x - \text{velocity}$$
$$v \; : \; y - \text{velocity}$$
$$c \; : \; \text{celerity}$$
$$g \; : \; \text{gravitational constant}$$

Given a coordinate transformation between the Cartesian coordinate system and general coordinate system

$$\xi = \xi(x, y), \;\; \eta = \eta(x, y),$$

we obtain the two-dimensional shallow water equations in a general coordinate

$$\hat{U}_t + \hat{F}_\xi + \hat{G}_\eta = 0.$$

Here

$$\hat{U} = \frac{1}{J} \begin{bmatrix} h \\ hu \\ hv \end{bmatrix},$$

$$\hat{F} = \frac{1}{J} \left(\xi_x \begin{bmatrix} hu \\ hu^2 + \frac{1}{2}gh^2 \\ huv \end{bmatrix} + \xi_y \begin{bmatrix} hv \\ hvu \\ hv^2 + \frac{1}{2}gh^2 \end{bmatrix} \right)$$

$$= \frac{1}{J} \left(U \begin{bmatrix} h \\ hu \\ hv \end{bmatrix} + \frac{1}{2}gh^2 \begin{bmatrix} 0 \\ \xi_x \\ \xi_y \end{bmatrix} \right),$$

$$\hat{G} = \frac{1}{J} \left(\eta_x \begin{bmatrix} hu \\ hu^2 + \frac{1}{2}gh^2 \\ huv \end{bmatrix} + \eta_y \begin{bmatrix} hv \\ hvu \\ hv^2 + \frac{1}{2}gh^2 \end{bmatrix} \right)$$

$$= \frac{1}{J} \left(V \begin{bmatrix} h \\ hu \\ hv \end{bmatrix} + \frac{1}{2}gh^2 \begin{bmatrix} 0 \\ \eta_x \\ \eta_y \end{bmatrix} \right),$$

where

$$J = \det \begin{bmatrix} \xi_x & \xi_y \\ \eta_x & \eta_y \end{bmatrix} = 1/\det \begin{bmatrix} x_\xi & x_\eta \\ y_\xi & y_\eta \end{bmatrix},$$
$$U = \xi_x u + \xi_y v,$$
$$V = \eta_x u + \eta_y v.$$

Using the following notation

$$M_\xi = \sqrt{\xi_x^2 + \xi_y^2},$$
$$\tilde{\xi}_x = \frac{\xi_x}{M_\xi},$$
$$\tilde{\xi}_y = \frac{\xi_y}{M_\xi},$$
$$\tilde{\theta}_\xi = \tilde{\xi}_x u + \tilde{\xi}_y v,$$

we obtain the Jacobian matrix

$$\frac{\partial \hat{F}}{\partial \hat{U}} = \begin{bmatrix} 0 & \xi_x & \xi_y \\ \xi_x(c^2 - u^2) - \xi_y uv & 2\xi_x u + \xi_y v & \xi_y u \\ -\xi_x uv + \xi_y(c^2 - v^2) & \xi_x v & \xi_x u + 2\xi_y v \end{bmatrix},$$

its corresponding eigenvalues are as follows

$$\lambda_1 = U - cM_\xi, \ \lambda_2 = U, \ \lambda_3 = U + cM_\xi,$$

its right eigenvectors are given by

$$R_1 = \begin{bmatrix} 1 \\ (\tilde{\theta}_\xi - c)\tilde{\xi}_x + \tilde{\xi}_y(\tilde{\xi}_y u - \tilde{\xi}_x v) \\ (\tilde{\theta}_\xi - c)\tilde{\xi}_y - \tilde{\xi}_x(\tilde{\xi}_y u - \tilde{\xi}_x v) \end{bmatrix}, \ R_2 = \begin{bmatrix} 0 \\ -\xi_y/\xi_x \\ 1 \end{bmatrix},$$

$$R_3 = \begin{bmatrix} 1 \\ (\tilde{\theta}_\xi + c)\tilde{\xi}_x + \tilde{\xi}_y(\tilde{\xi}_y u - \tilde{\xi}_x v) \\ (\tilde{\theta}_\xi + c)\tilde{\xi}_y - \tilde{\xi}_x(\tilde{\xi}_y u - \tilde{\xi}_x v) \end{bmatrix},$$

and its left eigenvectors have the following form

$$L_1 = \frac{1}{2c}\left((\tilde{\theta}_\xi + c), -\tilde{\xi}_x, -\tilde{\xi}_y\right),$$
$$L_2 = \left((\tilde{\xi}_y u - \tilde{\xi}_x v)\tilde{\xi}_x, -\tilde{\xi}_x\tilde{\xi}_y, \tilde{\xi}_x^2\right),$$
$$L_3 = -\frac{1}{2c}\left((\tilde{\theta}_\xi - c), -\tilde{\xi}_x, -\tilde{\xi}_y\right).$$

The eigenstructure for $\frac{\partial \hat{G}}{\partial \hat{U}}$ can be obtained similarly. We omit the explicit presentations to save space.

References

1. Bermudez, A., Vazquez, M.E.: Upwind methods for hyperbolic conservation laws with source terms. Comput. Fluids **23**, 1049–1071 (1994)
2. Cockburn, B., Shu, C.-W.: TVB Runge-Kutta local projection discontinuous Galerkin finite element method for conservation laws II: general framework. Math. Comput. **52**, 411–435 (1989)
3. Cosat, B., Don, W.S.: High order hybrid central-WENO finite difference scheme for conservation laws. J. Comput. Appl. Math. **204**, 209–218 (2007)
4. Hafez, M., Wahba, E.: Inviscid flows over a cylinder. Comput. Methods Appl. Mech. Eng. **193**, 1981–1995 (2004)
5. Harten, A.: Adaptive multiresolution schemes for shock computations. J. Comput. Phys. **115**, 319–338 (1994)
6. Hill, D.J., Pullin, D.I.: Hybrid tuned center-difference-WENO method for large eddy simulations in the presence of strong shocks. J. Comput. Phys. **194**, 435–450 (2004)
7. Jiang, G., Shu, C.-W.: Efficient implementation of weighted ENO schemes. J. Comput. Phys. **126**, 202–228 (1996)
8. Krivodonova, L., Xin, J., Remacle, J.-F., Chevaugeon, N., Flaherty, J.: Shock detection and limiting with discontinuous Galerkin methods for hyperbolic conservation laws. Appl. Numer. Math. **48**, 323–338 (2004)
9. LeVeque, R.J.: Finite volume methods for hyperbolic problems. Cambridge University Press, Cambridge (2002)
10. Li, G., Lu, C., Qiu, J.: Hybrid well-balanced WENO schemes with different indicators for shallow water equations. J. Sci. Comput. **51**, 527–559 (2012)

11. Li, G., Qiu, J.: Hybrid weighted essentially non-oscillatory schemes with different indicators. J. Comput. Phys. **229**, 8105–8129 (2010)
12. Nair, R.D., Thomas, S.J., Loft, R.D.: A discontinuous Galerkin transport scheme on the cubed sphere. Mon. Weather Rev. **133**, 814–828 (2004)
13. Nithiarasu, P., Zienkiewicz, O.C., Satyasai, B.V.K., Morgan, K., Codina, R., Vazquez, M.: Shock capturing viscosities for the general fluid mechanics algorithm. Int. J. Numer. Methods Fluids **28**, 1325–1353 (1998)
14. Noelle, S., Xing, Y.L., Shu, C.-W.: High-order well-balanced schemes. In: Puppo, G., Russo, G. (eds.) Numerical Methods for Balance Laws. Quaderni di Matematica (2010)
15. Pirozzoli, S.: Conservative hybrid compact-WENO schemes for shock-turbulence interaction. J. Comput. Phys. **178**, 81–117 (2002)
16. Qiu, J., Shu, C.-W.: A comparison of troubled-cell indicators for Runge-Kutta discontinuous Galerkin methods using weighted essentially nonoscillatory limiters. SIAM J. Sci. Comput. **27**, 995–1013 (2005)
17. Shu, C.-W.: Essentially non-oscillatory and weighted essentially non-oscillatory schemes for hyperbolic conservation laws, NASA/CR-97-206253, ICASE Report NO.97-65
18. Shu, C.-W.: High order weighted essentially nonoscillatory schemes for convection dominated problems. SIAM Rev. **51**, 82–126 (2009)
19. Shu, C.-W., Osher, S.: Efficient implenmentiation of essentially non-oscillatory shock-capturing schemes. J. Comput. Phys. **77**, 439–471 (1988)
20. Shu, C.-W., Osher, S.: Efficient implenmentiation of essentially non-oscillatory shock-capturing schemes, II. J. Comput. Phys. **83**, 32–78 (1989)
21. Shu, C.-W., Zang, T.A., Erlebacher, G., Whitaker, D., Osher, S.: High-order ENO schemes applied to two- and three-dimensional compressible flow. Appl. Numer. Math. **9**, 45–71 (1992)
22. Toro, E.F.: Shock-capturing methods for free-surface shallow flows. Wiley, Chichester (2001)
23. Toro, E.F.: Riemann solvers and numerical methods for fluid dynamics, 3rd edn. Springer, Berlin (2009)
24. Xing, Y., Shu, C.-W.: High order finite difference WENO schemes with the exact conservation property for the shallow water equations. J. Comput. Phys. **208**, 206–227 (2005)
25. Zhu, H., Qiu, J.: Adaptive Runge-Kutta discontinuous Galerkin methods using different indicators: one-dimensional case. J. Comput. Phys. **228**, 6957–6976 (2009)